Contribution of parsec-scale material on to the polarized X-ray spectrum of type 1 Seyfert galaxies

F. Marin, M. Dovčiak, E.S. Kammoun

Monthly Notices
of the
ROYAL ASTRONOMICAL SOCIETY

MNRAS **478,** 950–960 (2018)
Advance Access publication 2018 April 27

doi:10.1093/mnras/sty1062

Contribution of parsec-scale material on to the polarized X-ray spectrum of type 1 Seyfert galaxies

F. Marin,[1]★ M. Dovčiak[2] and E. S. Kammoun[3]

[1]*Université de Strasbourg, CNRS, Observatoire Astronomique de Strasbourg, UMR 7550, F-67000 Strasbourg, France*
[2]*Astronomical Institute of the Academy of Sciences, Boční II 1401, CZ-14100 Prague, Czech Republic*
[3]*SISSA, via Bonomea 265, I-34135 Trieste, Italy*

Accepted 2018 April 23. Received 2018 April 13; in original form 2018 March 9

ABSTRACT

Type 1 radio-quiet active galactic nuclei (AGN) are seen from the polar direction and offer a direct view of their central X-ray engine. If most of X-ray photons have travelled from the primary source to the observer with minimum light–matter interaction, a fraction of radiation is emitted at different directions and is reprocessed by the parsec-scale equatorial circumnuclear region or the polar outflows. It is still unclear how much the polarization expected from type 1 AGN is affected by radiation that have scattered on the distant AGN components. In this paper, we examine the contribution of remote material on to the polarized X-ray spectrum of type 1 Seyfert galaxies (Seyfert-1s) using radiative transfer Monte Carlo codes. We find that the observed X-ray polarization strongly depends on the initial polarization emerging from the disc–corona system. For unpolarized and parallelly polarized photons (parallel to the disc), the contribution is negligible below 3 keV and tends to increase the polarization degree by up to one percentage points at higher energies, smoothing out the energy-dependent variations of the polarization angle. For perpendicularly polarized corona photons, the addition of the circumnuclear scattered (parallel) component adds to the polarization above 10 keV, decreases polarization below 10 keV and shifts the expected 90° rotation of the polarization angle to lower energies. In conclusion, we found that simulations of Seyfert-1s that do not account for reprocessing on the parsec-scale equatorial and polar material are under- or overestimating the X-ray polarization by 0.1–1 percentage points.

Key words: galaxies: active – polarization – radiative transfer – relativistic processes – scattering – X-rays: general.

1 INTRODUCTION

In active galactic nuclei (AGN) that are not dominated by synchrotron processes in the form of failed or extended jets, all observed X-ray fluxes originate from the vicinity of their central supermassive black hole (SMBH). It is accepted that the SMBH accretion disc emits thermal ultraviolet photons that are reprocessed to the X-rays by Comptonization processes in a hot corona lying above (Haardt & Maraschi 1991, 1993) or maybe inside the disc (Done et al. 2012). The geometry, spatial extension, composition, and temperature of this corona have been investigated by many authors. The most recent observational constraints have been achieved in the hard X-ray spectrum of AGN by *NuSTAR* that helped to improve our knowledge on the hot corona (Fabian et al. 2015, 2017; Matt et al. 2015; Tortosa et al. 2018). Current constraints tend to picture the corona as compact, being only a few gravitational radii (r_G) in size, with an anticorrelation between the coronal optical depth and the coronal temperature (Tortosa et al. 2018). Spectral timing and reverberation studies also suggest a compact corona, most likely situated on the disc axis and located within 3–10r_G from the central SMBH (Zoghbi et al. 2010; Emmanoulopoulos et al. 2014; Gallo et al. 2015, but see also Dovčiak & Done 2016 for the minimum X-ray source size of the on-axis corona in AGN). X-ray microlensing analyses of lensed quasars also suggest that the X-ray emitting region is compact, having a half-light radius $\leq 6r_G$ (Chartas et al. 2009; Mosquera et al. 2013; Reis & Miller 2013). However, the geometrical aspect of the corona is probably the most complicated aspect to study since spectroscopy has a limited sensitivity to the morphology of the emitting medium (Wilkins & Fabian 2012). Polarization, however, can distinguish more easily between different geometries as the polarization of light is strongly influenced by morphological and composition variations (Dovčiak et al. 2008; Schnittman & Krolik 2010; Marin & Tamborra 2014). The launch of the *Imaging X-ray*

★ E-mail: frederic.marin@astro.unistra.fr

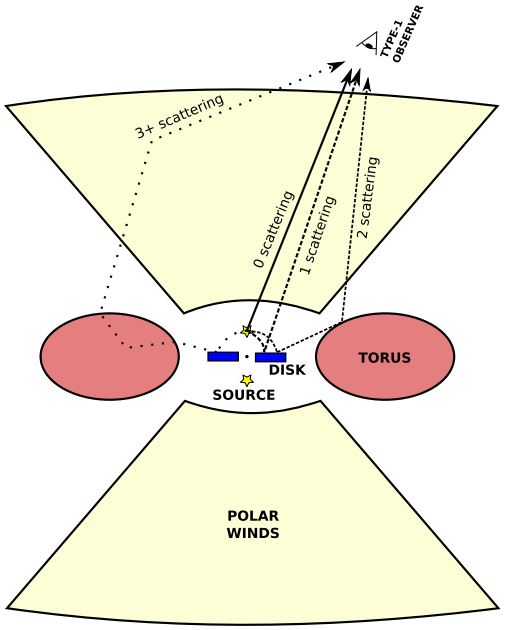

Figure 1. Artist representation of the AGN model. Scales have been exaggerated for better visualization of the inner components. The point-like coronas are represented with yellow stars, the cold accretion disc is in blue, the gaseous torus in red, and the polar outflows in primrose yellow. The photon trajectories are bend close to the central SMBH and radiation have multiple potential targets for interaction, depending upon the energy of the photon and Compton thickness of the material. The solid line represents the direct flux from the source (no scattering at all) and the other lines represent different possible radiation paths with different numbers of scattering.

Polarimetry Explorer (*IXPE*) in 2021 is expected to revolutionize our understanding of the central engine of AGN by probing the geometry of the corona for the first time, among other fascinating topics (Weisskopf et al. 2016).

In order to predict the degree and angle of X-ray polarization we expect from radio-quiet AGN, proactive Monte Carlo simulations are necessary to explore in great details the radiative and reprocessing environment of SMBH (see e.g. Connors, Stark & Piran 1980; Haardt & Matt 1993; Massaro et al. 1993; Dovčiak, Karas & Matt 2004a). The central engine, consisting of a potential well, an accretion disc, and a lamppost corona, is usually explored individually, disregarding any contribution from material above a few hundreds of gravitational radii. The processes occurring close to the singularity being complex due to special and general relativity, it is traditional to isolate the central AGN engine to estimate the X-ray polarization of type 1 AGN (see e.g. Dovčiak et al. 2004a). This, of course, cannot work for type 2 AGN, where the primary source is hidden behind a Compton-thick reservoir of cold matter situated at parsec-scales distances (see a modern AGN illustration in Marin 2016, or a simplified scheme in Fig. 1). The X-ray polarization emerging from type 2 AGN is strongly dominated by polar scattering inside the AGN outflows at soft X-ray energies, but signatures of the disc–corona system may be detected in the hard band if the equatorial torus material has a Compton thickness largely inferior to 10^{25}atm cm^{-2} (Marin et al. 2018). The parsec-scale AGN components are thus important to evaluate the X-ray properties of AGN, such as demonstrated by e.g. Ghisellini, Haardt & Matt (1994) for spectroscopy and spectral energy distribution purposes. Yet, the contribution of those distant AGN components to the X-ray polarization spectrum of type 1 Seyferts is not known.

This is the goal of our study: to couple the emission and scattering of X-ray photons by the disc–corona system governed by strong gravity effects to absorption, re-emission, and scattering processes happening at parsec-scale distances from the potential well. This investigation is a follow-up of the work from Marin et al. (2018), where the same model and same codes were applied to estimate the X-ray polarization signal of type 2 AGN. In this paper, we check whether the parsec-scale torus and polar winds have an impact on the expected polarization of type 1 AGN. If so, we evaluate how much of the signal is diluted or enhanced. To do so, we briefly remind the reader about the model and Monte Carlo codes used in our simulations in Section 2. We then present our results in Section 3, where different initial polarization states of the corona are investigated. In Section 4 we explore how much the Compton thickness of the outflows, and circumnuclear region influence our results. We conclude our paper in Section 5 by quantifying the excess or deficiency of X-ray polarization estimated by previous type 1 AGN simulations.

2 MODELLING

Our modelling is exactly the same as previously described in details in Marin et al. (2018). The sole difference is that we are looking at a typical type 1 inclination ($\sim$20° from the polar axis of the model) rather than at a type 2 orientation. In the following, we remind the reader about the Monte Carlo codes used and the geometry and composition of the AGN model.

2.1 The radiative transfer codes

To compute the radiative transfer of photons emitted from a spherical corona situated above the accretion disc in a lamppost geometry, we used the KY code presented in Dovčiak, Karas & Yaqoob (2004b). KY is a relativistic ray tracing code that computes the time evolution of a local spectrum seen by a distant observer. The code includes the full set of Stokes parameters to compute polarization, accounts for a variety of inclinations, black hole masses, corona locations, and potential orbiting clouds. Reprocessing in the disc is calculated with the Monte Carlo multiscattering code NOAR (Dumont, Abrassart & Collin 2000) that computes the reflected flux including the iron fluorescent Kα and Kβ lines. The single-scattering approximation (Chandrasekhar 1960) is used for the local polarization of the reflected continuum component, while the line flux is assumed to be unpolarized.

Once the radiation field emerging from the disc–corona system computed, we inject the photons into the Monte Carlo code STOKES. Designed by Goosmann & Gaskell (2007) and developed by Marin et al. (2012b), Marin, Goosmann & Gaskell (2015), and Rojas Lobos et al. (2018) and Marin (2018), STOKES is a Monte Carlo code that simulates light reprocessing in any three-dimensional environment. The code can compute the effect of multiple scattering and radiative coupling between a large number of media, from the near-infrared to the hard X-ray band. All the necessary absorption, re-emission, and scattering physics are included in the code to cover such a large waveband (Marin & Goosmann 2014). Escaping photons are finally recorded by a spherical web of virtual detectors at all polar and azimuthal directions. Using the output of KY as an input for STOKES, we are thus able to provide a consistent picture of the X-ray photons that emerge from the few gravitational radii around the central SMBH to reach the parsec-scale regions that constitute the external envelope of AGN.

2.2 The AGN model

Our AGN model is presented in Fig. 1. It consists of a central SMBH of $\sim 10^8$ $M_\odot$ that represents the median value of the black hole mass distribution observed in large radio-quiet Seyfert catalogues by Woo & Urry (2002). The dimensionless spin parameter of the black hole is either fixed to 0 (non-rotating Schwarzschild case) or 1 (maximally rotating Kerr case). Around the potential well we set a geometrically thin, optically thick accretion disc. Its inner radius is fixed by the spin value and its outer radius extends up to $1000r_G$, where strong gravity effects are no longer necessary. Since we do not consider super-Eddington flows that would require slim/flared discs (Sądowski et al. 2011), our disc is modelled using the usual slab geometry (e.g. Dovčiak et al. 2004a). The standard thin disc is uniformly filled with cold material, a valid scenario as long as the incident X-ray flux is smaller than or comparable with the soft thermal flux generated intrinsically in the disc (Nayakshin & Kallman 2001). New tables for moderately and highly ionized discs are currently computed (Goosmann et al., in preparation). The hot corona in our model is set along the rotation axis of the disc at a height of $3r_G$. The point-like corona emits a power-law X-ray spectrum with a photon index $\Gamma = 2$ and initial photons can have any intrinsic polarization.

Surrounding the central engine, an obscuring circumnuclear region usually referred to as the 'torus' prevents radiation from escaping the equatorial plane. The half-opening angle of the torus is set to 60° from the polar axis, so the line-of-sight of a polar observer is unobscured by the gaseous medium. The inner radius of the cold material is fixed to 0.01 pc from the centre of the model according to reverberation mapping data (Suganuma et al. 2006; Vazquez et al. 2014), and extends up to 5 pc. We also fixed the hydrogen column density along equatorial plane to 10^{24}atm cm^{-2}. The torus is thus at the limit between Compton-thin and Compton-thick categories and can be representative of both AGN classes (Georgakakis et al. 2017). Finally, along the pole, we added outflowing winds collimated by the torus funnel. The winds extend 60° from the polar axis and are composed of neutral gas in a Compton-thin regime (10^{21}atm cm^{-2}). Those winds correspond to the narrow-line region (NLR) that extends over several kiloparsecs in nearby AGN before mixing with the interstellar medium (Wang, Xu & Wei 2016). The NLR is characterized with little absorption features in the X-ray band and can be simply modelled using cold gaseous material (Wang et al. 2016). More ionized material, such as the warm absorber region (Reynolds & Fabian 1995; Porquet & Dubau 2000) or the ultrafast outflows (Tombesi et al. 2010, 2011, 2012) are not explored here since they would not strongly contribute to the expected X-ray polarization continuum of AGN (Marin et al. 2018). We thus simplify our model by accounting for only one large polar region. The wind base is located at a radial distance of 0.1 pc from the centre of the model (Taniguchi & Anabuki 1999) and extends up to 25 pc, before mixing with the interstellar medium.

In total, there are three different targets for radiation to interact with: the accretion disc, the torus, and the outflows. The resulting polarization emerging from each isolated component is presented in Fig. 2. If the primary source of photons (the corona) has no intrinsic polarization, it will only dilute the observed polarized flux. However, if it is intrinsically polarized by inverse Compton scattering of disc photons, the corona will also play a role in determining the polarization at infinity. In our model, we see that the direct flux of photons coming from the corona is polarized at a constant level that is independent of energy. Not all primary photons directly reach the observer; a substantial fraction of corona radiation is bent towards the disc by relativistic effects. Photons scattered by the disc keep

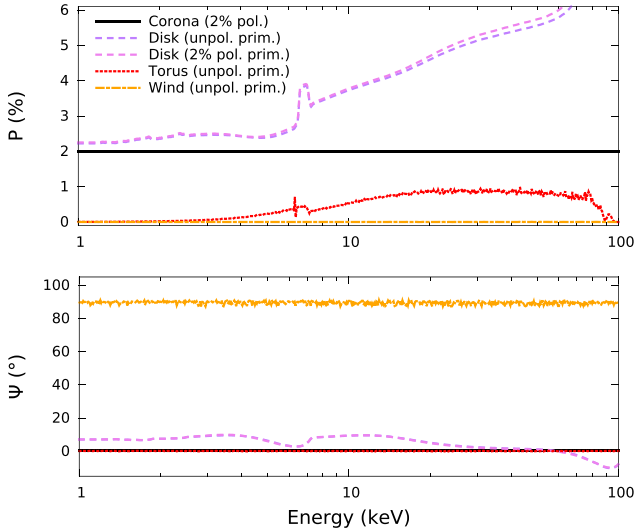

Figure 2. X-ray polarization degree (top panel) and position angle (bottom panel) from the different components of our AGN model. The inclination of the observer is 20° and the photon source is either unpolarized or polarized at 2 per cent level. Solid line (black): polarization from the photons originating from the corona (no scatterings); dashed line (purple): polarization scattered from the disc using an unpolarized primary; dashed line (violet): polarization scattered from the disc using a 2 per cent polarized primary; dotted line (red): polarization scattered from the torus using an unpolarized primary; and dot–dashed line (orange): polarization scattered from the polar winds using an unpolarized primary.

memory of their initial polarization but, according to the scattering position with respect to the potential well and the energy of the photon, their polarization degree and angle will change. We show two different cases where the initial polarization is either 0 or 2 per cent. Interestingly, the two scattering-induced polarization levels are very similar. Our choice to use a 2 per cent polarized primary is driven by the fact that a similar level of polarization (for a viewing angle of 20°) is produced by reflection from the disc. This allows us to model the polarization of a central engine that is not entirely dominated by the polarization of the corona. We also point out that the Compton hump polarization, resulting from corona–disc scattering, can be quite high in both cases (see e.g. fig. 6 in Dovčiak et al. 2011), and it strongly depends on the height of the primary source, the inclination of the observer, and the spin of the black hole. Looking at the polarization produced by the parsec-scale components, we see that scattering of unpolarized photons by the torus produces a polarization degree of 0.1–1.2 per cent with a constant polarization angle of 0°. On the contrary, forward scattering in the polar winds produces almost no polarization and its position angle is perpendicular to the polarization angle from the torus. For both spectra, we used an unpolarized primary to better isolate the true polarization resulting from scattering on to the parsec-scale components.

Polarization being a vectorial quantity, it is not possible to simply add the contribution of each element to create the final polarized spectrum. The polarization emerging from a model where several components are coupled is thus not easily estimated by linear scaling or approximations without prior knowledge of the total AGN polarization. The impact of radiative coupling between the various AGN constituents is precisely what we intend to explore in this paper. For all the simulations we present,

the observer's inclination is fixed to a typical type 1 value of 20°.

2.3 Polarization of the primary source

Our primary source is a point-like corona above the accretion disc. Its physical size and composition are not relevant to this paper since, in the following, all our AGN spectra will be compared to the spectra emerging from the disc–corona system. The differences we will detect can be extrapolated for all different corona properties. The corona itself may, however, emit different flavours of photons. Either the interaction of ultraviolet photons with the hot electrons produces unpolarized X-ray photons, or the outgoing photons are carrying a substantial polarization degree with a given polarization position angle. Detecting those polarization levels is extremely important to determine the composition, temperature, and geometry of the corona and it will be an important target for *IXPE* (Marin & Tamborra 2014; Weisskopf et al. 2016).

In this paper, similarly to Marin et al. (2018), we investigate three different coronal polarizations. In Fig. 3, the input photons are not polarized. Coronal radiation travels along photons null geodesics before escaping towards the observer or impacting the disc. The local polarization is computed and the photon can either be absorbed, scatter several times in the disc, or escape. The strong gravity effects influence the polarization position angle of radiation as it travels close to the potential well (Connors et al. 1980). The differences we see in Fig. 3 between a Schwarzschild and a Kerr model are due to the radius of the innermost stable circular orbit that is six times smaller in the latter case. The receding and approaching parts of the disc contributing differently to the sum of polarization also explain the differences in terms of polarization degree P and polarization angle Ψ. Details of the energy-dependent variations of the spectra are extensively given in Marin et al. (2018).

In Fig. 4, we show the same modelling of the disc–corona system but with a 2 per cent polarized primary. While the true initial polarization of X-ray coronas is still unknown, as it depends on its geometry, optical depth, temperature, and the inclination of the whole system, recent numerical simulations favour low polarizations degrees, of the order of a few per cent (Schnittman & Krolik 2010; Matt & Tamborra 2018). As explained in the previous section, we choose a 2 per cent primary polarization, a value that has the particularity of being close to that of the polarization produced by the disc at an inclination of 20°. Thus, we can investigate the specific case where the polarization signal from the corona is not dominating the polarization from the disc. The left-hand column shows an initial polarization position angle of the primary source perpendicular to the disc surface, while the right-hand column is for parallel polarization (polarization angle parallel to the disc). We define a parallel polarization angle to be 0° and a perpendicular polarization angle to be 90°. We caution the reader that this is a different convention than what was used in Marin et al. (2018). We changed the convention in order to be in agreement with other polarization codes. The most striking difference between a polarized and an unpolarized source is the degree of polarization. At low energies, where photoabsorption in the disc dominates, the degree of polarization is the same as the corona input polarization. However, once the disc starts to reflect X-ray light, the polarization either increases or decreases depending on the polarization angle of input radiation. Scattering inside the disc tends to give parallel polarization angles, so if the input photons are already parallelly polarized the resulting polarization degree increases. Otherwise there

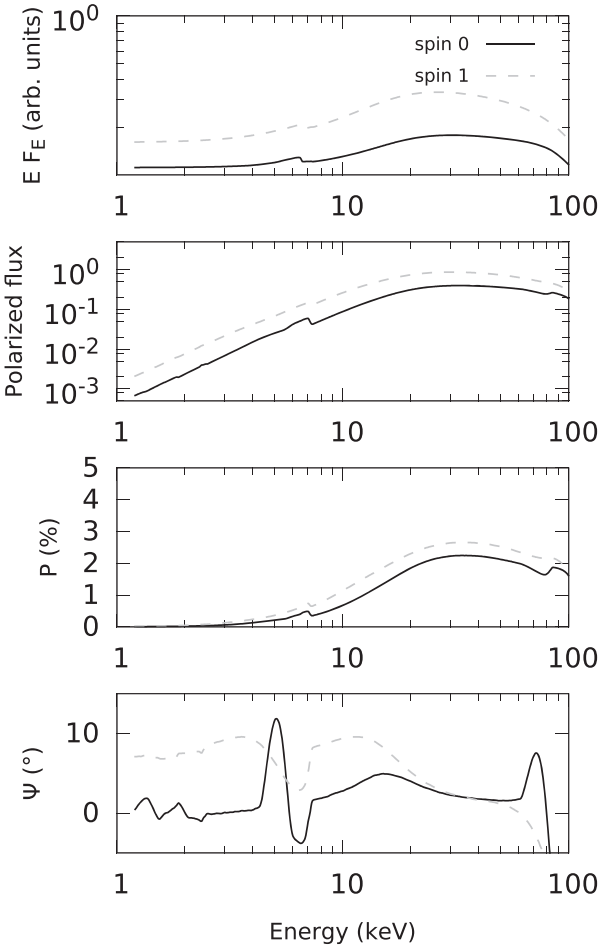

Figure 3. X-ray flux (F_E is energy flux at energy E), polarized flux, polarization degree P, and polarization position angle Ψ seen by an observer at infinity, resulting from an elevated point-like corona that irradiates an accretion disc inclined by 20°. The source is unpolarized. The variation in P and Ψ is due to general relativistic effects that will induce a parallel transport of the polarization angle along geodesics, plus the scattering and re-emission of photons from the cold accretion matter. Two flavours of black holes are shown: a non-spinning Schwarzschild black hole (black solid line) and a maximally spinning Kerr black hole (grey dashed line).

is orthogonality between the two vectorial components, decreasing the net polarization degree. This is the reason why the polarization angle rotates between 90° and 0° between 10 and 20 keV. Finally, the strong feature appearing at very high energies is a numerical artefact caused by the truncated power law and the energy shift of photons that affect energies higher than 70 keV and create empty bins.

3 RESULTS

The results presented in Figs 3 and 4 only account for the central engine. The contribution of the parsec-scale AGN components is disregarded. Those results are typically used to predict the degree and angle of polarization a future X-ray polarimetric satellite will observe in the case of type 1 AGN after the addition of Galactic absorption along the line-of-sight. In this section, we include the central AGN engine inside a larger model with a torus and polar

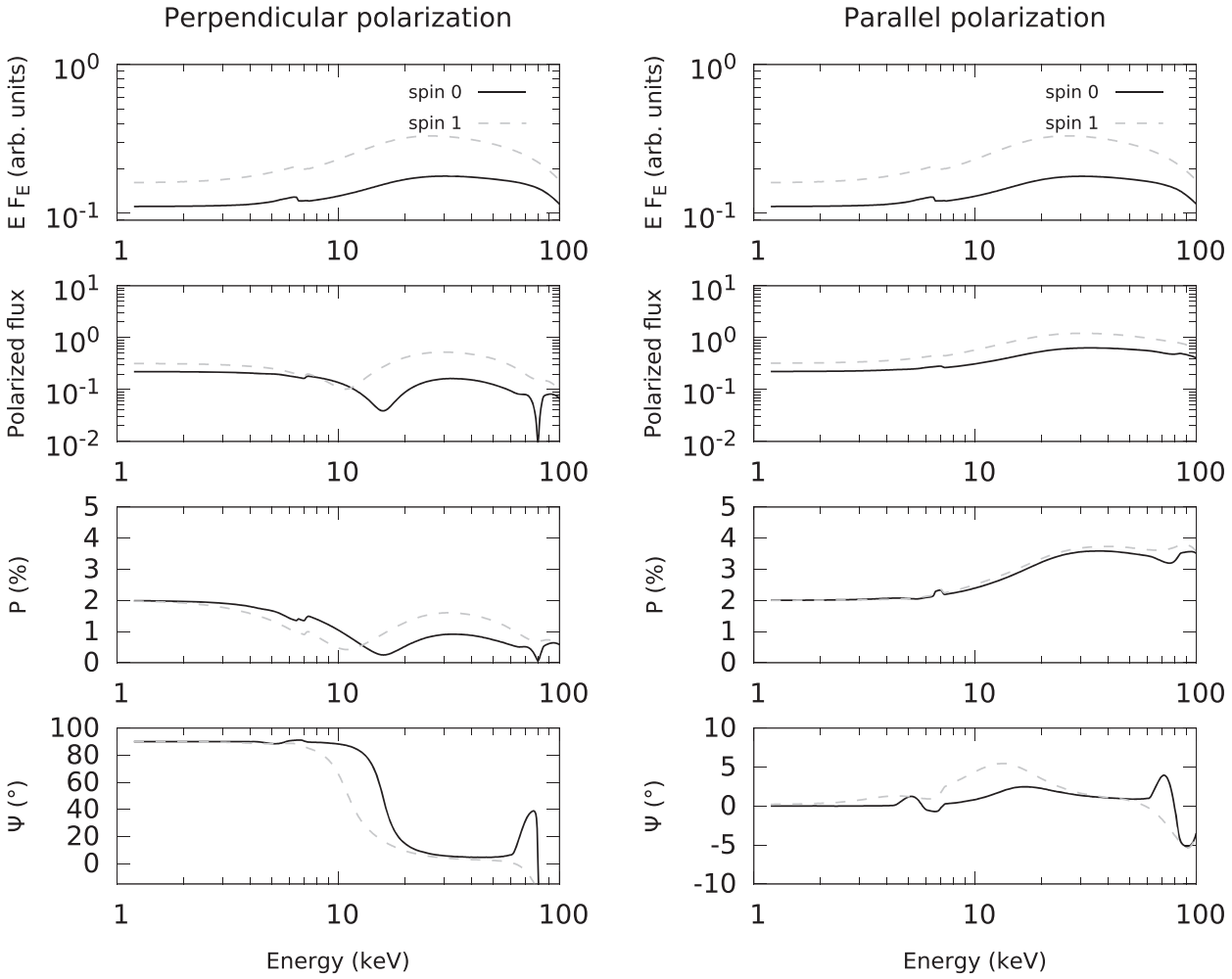

Figure 4. X-ray flux (F_E is energy flux at energy E), polarized flux, polarization degree P, and polarization position angle Ψ seen by an observer at infinity, resulting from an elevated point-like corona that irradiates an accretion disc inclined by 20°. The initial polarization is set to 2 per cent with a parallel or a perpendicular polarization angle (right- and left-hand column, respectively). The variation in P and Ψ is due to general relativistic effects that will induce a parallel transport of the polarization angle along geodesics, plus the scattering and re-emission of photons from the cold accretion matter. Two flavours of black holes are shown: a non-spinning Schwarzschild black hole (black solid line) and a maximally spinning Kerr black hole (grey dashed line).

winds (see Fig. 1). By doing so, we can estimate how different the polarimetric results are once the contribution of all AGN parts is accounted for.

3.1 Type 1 spectra with an unpolarized primary source

We start our investigation with a model where the primary source emits photons that are randomly polarized (the resulting net polarization is thus null). We see from Fig. 5 (Schwarzschild case, left-hand column) that the X-ray intensity spectrum of the AGN model is not strongly affected by the presence of the torus and winds. There is slightly more absorption in the soft X-ray band with respect to the input disc–corona spectrum (in dashed line). This extra absorption is similar to what we observe when we take into account Galactic absorption (Zamorani et al. 1988) and is due to the Compton-thin polar winds. The very soft X-ray photons are absorbed by the cold material, while higher energy photons pass through without interacting. We also detect the presence of fluorescence lines that originate from the winds and torus, with a narrow Fe Kα dominating the spectrum at 6.4 keV. This narrow component is an almost ubiquitous feature in the X-ray spectra of AGN and, in our case, mainly originates from the neutral material located in the molecular torus (see also Ricci et al. 2014). There are no absorption lines since we do not model the warm absorber region. The X-ray polarized spectrum (second panel from the top) appears to be very similar to the input polarized spectrum, being marginally higher due to extra scattering on the parsec-scale components. The polarized flux being the multiplication of the intensity spectrum and the polarization degree, it is then logical to observe that the input corona–disc system polarization is lower than the final full AGN model polarization degree P. If the difference is negligible in the soft band ($E < 3$ keV), the AGN polarization degree is twice higher in the 3–10 keV band, increasing by 0.1–0.5 percentage points. The difference is even higher in the Compton hump where the polarization degree increases from 2 to 3 per cent. Multiple scatterings between the disc–corona system and the parsec-scale components play a not-so-negligible role in determining the true X-ray polarization expected from type 1 AGN. The main contributor to this additional polarization is the torus, which produces an additional parallelly polarized component that affects the whole energy band. The differences in terms of polarization position angle Ψ are less important as the energy-dependent variations of Ψ remain the same.

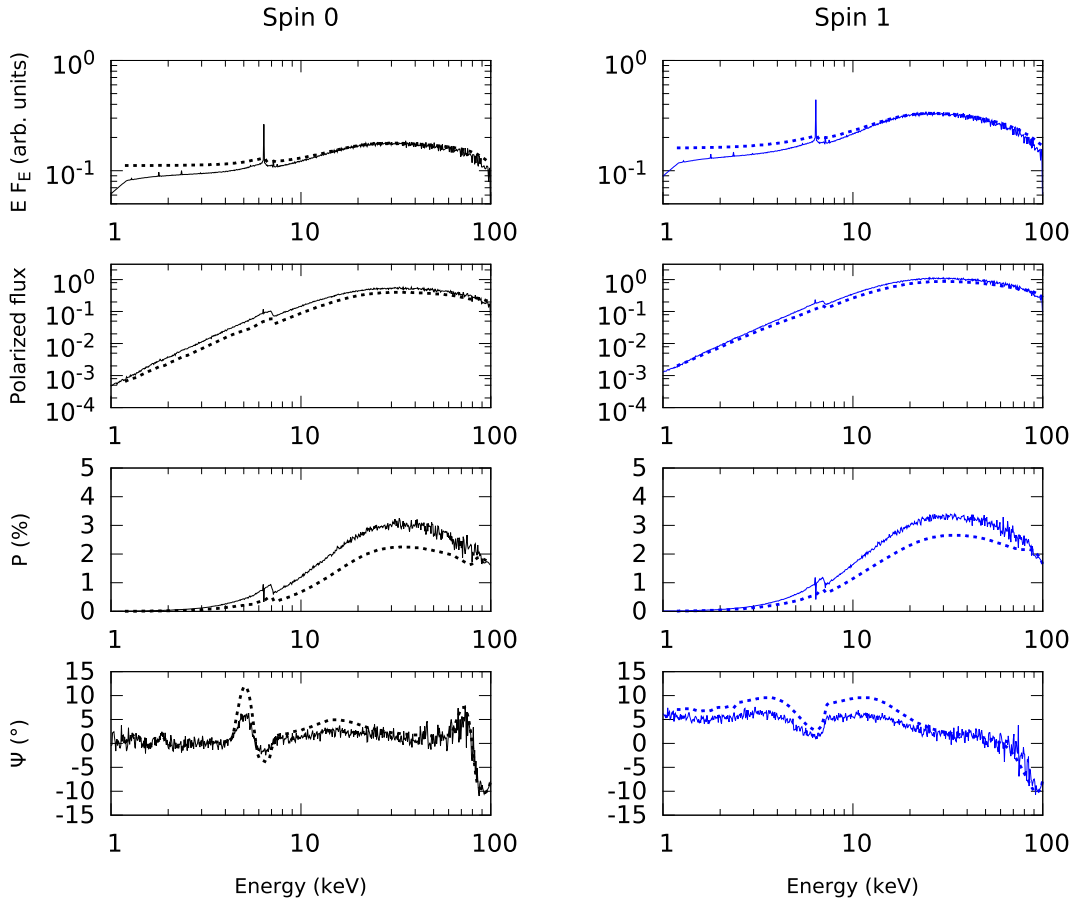

Figure 5. X-ray flux (F_E is energy flux at energy E), polarized flux, polarization degree, and polarization position angle for a type 1 AGN with a Compton-thick torus ($n_{\mathrm{H_{torus}}} = 10^{24}$atm cm^{-2}) and Compton-thin absorbing polar winds ($n_{\mathrm{H_{wind}}} = 10^{21}$atm cm^{-2}). See text for additional details about the model components. The input corona spectrum is unpolarized and shown in dotted line.

Only the intensity of the variations is smoothed out since scattering by the equatorial parsec-scale component tends to fix the polarization angle to 0°.

The case is very similar for a Kerr black hole (Fig. 5, right-hand column), with the exception of the intensity spectrum that shows higher fluxes but with the same absorption levels in the soft X-ray band. The principal method to distinguish between a non-rotating and a maximally rotating black hole relies on the energy-dependent variations of Ψ, which are conserved despite the addition of the torus and polar outflows. It is thus safe to say that adding parsec-scale components do not modify past predictions if the coronal photons are unpolarized. The parsec-scale components only uplift previous estimations of the X-ray polarization degree we expect, which is more favourable for observations.

3.2 Type 1 spectra with a (2 per cent parallel) polarized primary source

We continue our tests by setting the initial polarization of the primary source to 2 per cent, with a polarization position angle parallel to the disc. The resulting intensity spectrum for both the Schwarzschild and Kerr cases (Fig. 6, top figures) is completely insensitive to the polarization state of the corona, such as already mentioned in the Introduction. Only the polar outflows have an impact on the soft part of the spectra, similarly to the previous model (Fig. 5). The polarized flux is, however, different since the spectra are lower in intensity than the input ones in the soft band. However the AGN polarized spectra become higher than the corona–disc polarized spectra at $E \geq 10$ keV. Since we observe that the polarization degree is the same between the input and output spectra (Fig. 6, third panels from the top), the extra absorption brought by the polar outflows explains the behaviour of the polarized spectra in the soft part. The initial polarization of the corona dominates the soft photon flux since most of the detected radiations have travelled directly from the source to the observer. In the case of the hard band, extra Compton scattering is responsible for higher final polarization degrees, 0.5–1 percentage points higher at 30 keV than the input polarization, and thus drives the polarized fluxes to higher values. In comparison to a model with unpolarized primary photons, we find an overall higher polarization degree associated with the same energy-dependent variations of Ψ. However, in this case, the differences between the polarization position angle of the models with and without parsec-scale AGN components are completely negligible.

3.3 Type 1 spectra with a (2 per cent perpendicular) polarized primary source

The last parametrization of the corona input polarization retains the same degree of polarization but changes the orientation of the

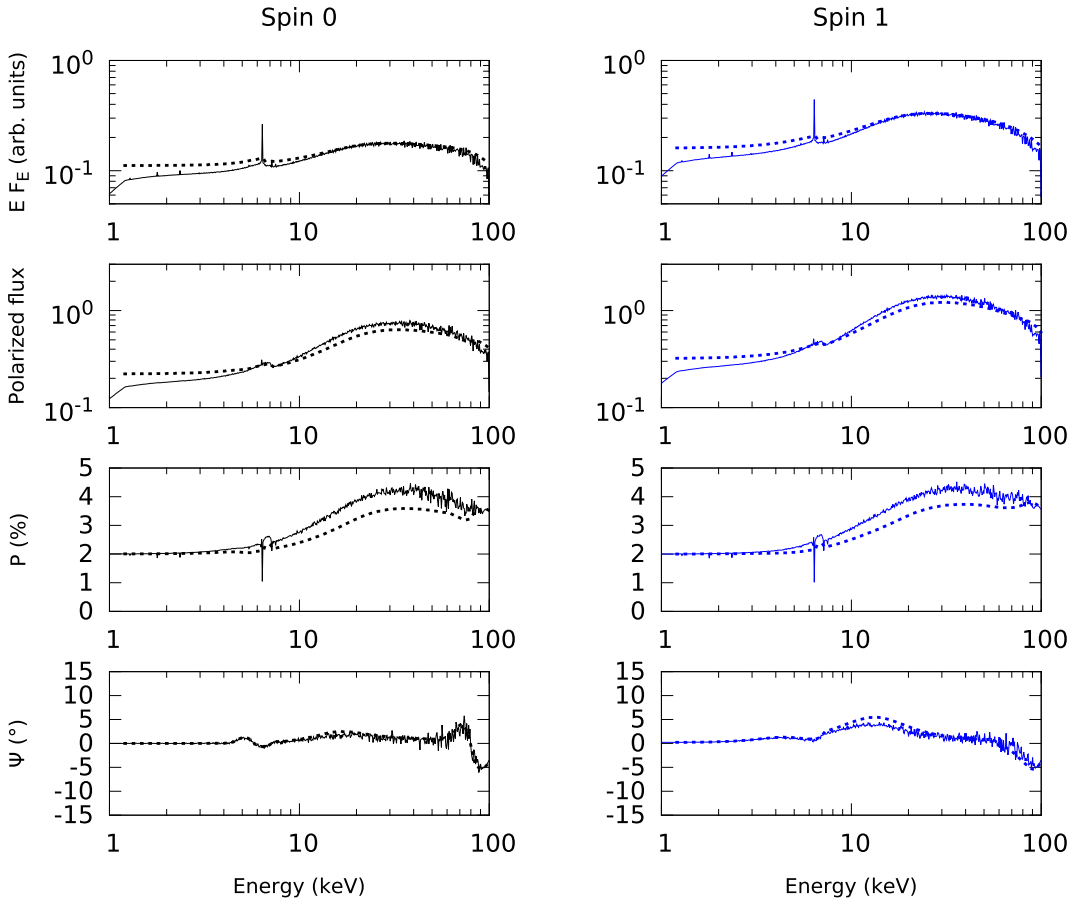

Figure 6. X-ray flux (F_E is energy flux at energy E), polarized flux, polarization degree, and polarization position angle for a type 1 AGN with a Compton-thick torus ($n_{\mathrm{H_{torus}}} = 10^{24}$atm cm^{-2}) and Compton-thin absorbing polar winds ($n_{\mathrm{H_{wind}}} = 10^{21}$atm cm^{-2}). The input corona spectrum is 2 per cent parallelly polarized and shown in dotted line.

polarization position angle. Ψ is now perpendicular to the accretion disc. We observe that this different polarization set-up again has no influence on to the total intensity spectra of both the Schwarzschild and Kerr cases (Fig. 7, top figures). The polarized spectra (second figures from the top) are however quite different with respect to the previous realizations. There is a sharp dip in the polarized spectra at different energies between the disc–corona system (dashed line) and the full AGN model (solid line). The differences are due to the polarization angle of radiation. We see from the Ψ energy dependence that there is a rotation of the polarization position angle, such as already shown in Section 2.3. However, the energy at which the transition occurs is different: it happens at lower values, typically 10 keV. This variation is predominantly due to the extra scattering components. Since there is an additional flux coming from scattering on to the equatorial torus (that gives rise to parallel polarization), the amount of parallel polarization is larger in the case of a full AGN model than for the isolated central engine. The competition between parallel and perpendicular polarization is stronger and has the effect of moving the energy at which the transition occurs to lower values. The transition is also sharper. The dominance of perpendicular radiation from the primary source in the soft band explains why the final polarization is lower than the 2 per cent input polarization. However, once Ψ has rotated, the final degree of polarization increases to higher values than the initial spectra. We also find a 0.5–1 percentage points increase of P in the Compton hump, similarly to the previous cases.

4 DISCUSSION

It appears that if the type 1 intensity spectrum of AGN is affected by the presence of an equatorial torus and polar outflows, the former imprinting the spectrum with strong emission lines and the latter absorbing soft X-ray photons, it is completely insensitive to the polarization of the primary source. This conclusion is not new, since many authors have explored the effect of parsec-scale AGN components on to the X-ray intensity spectrum of AGN (e.g. Ghisellini, Haardt & Matt 1994; Schurch & Done 2007; Schurch, Done & Proga 2009; Ricci et al. 2014). What is innovative, is that the impact of those parsec-scale media has been demonstrated to alter the expected polarization signal from the disc–corona system even in type 1 orientations. The presence of additional scattering targets that are not within the influence zone of the central potential well may change the expected degree of polarization in different ways. If the X-ray photons produced in the hot corona are unpolarized or polarized parallelly to the accretion disc, we expect higher polarization degrees due to higher probabilities of scattering events. In particular the Compton hump shows a polarization degree on av-

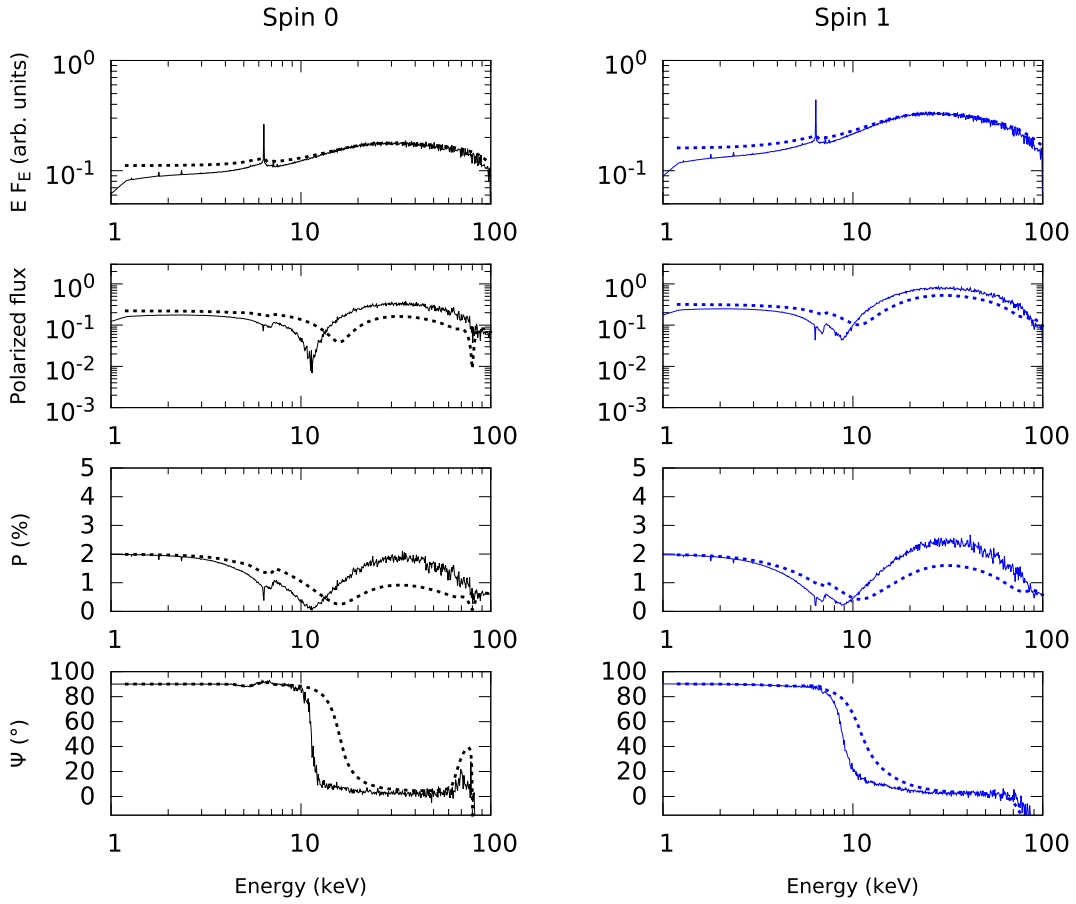

Figure 7. X-ray flux (F_E is energy flux at energy E), polarized flux, polarization degree, and polarization position angle for a type 1 AGN with a Compton-thick torus ($n_{\rm H_{torus}} = 10^{24}$atm cm^{-2}) and Compton-thin absorbing polar winds ($n_{\rm H_{wind}} = 10^{21}$atm cm^{-2}). The input corona spectrum is 2 per cent perpendicularly polarized and shown in dotted line.

erage 0.5–1 percentage points higher than expected. The soft band ($E \leq 10$ keV) sees its polarization degree changing by a fraction of a per cent, depending on the input corona polarization degree. The polarization angle is not affected. In the case of a source of perpendicularly polarized photons, we find that simulations that only account for an isolated disc–corona system usually overestimate the true polarization degree in the soft band and underestimate it in the Compton hump. Additionally, the rotation of the polarization angle between the soft and the high-energy band is shifted towards lower energies due to the enhanced production of parallel photons by the torus.

We have thus proven that parsec-scale AGN components are important when estimating the true X-ray polarization we expect from type 1 radio-quiet AGN. Varying the parametrization of the disc–corona system, such as the height of the corona or its initial polarization degree, will change the polarization from the central engine but not the impact of the distant components. First-order rescaling of the results is possible in those cases. On the other hand, polarization is sensitive to the inclination of the system, together with the geometry of the different components. It is then important to run new simulations in order to estimate the X-ray polarization from a complete AGN model that is viewed at a different orientation or that is modelled using different geometrical components. Finally, it is still unclear if varying the Compton thickness of the torus and winds could drastically change our results. We thus examine this question in the following subsections.

4.1 Impact of torus thickness

In Fig. 8, we present the same AGN model as in Section 6, i.e. with a 2 per cent parallel polarization primary source on top of a maximally rotating SMBH (spin 1), but we vary the hydrogen column density of the circumnuclear region. We examine the Compton-thin hypothesis ($n_{\rm H_{torus}} = 10^{23}$atm cm^{-2}, black line), the transition value between Compton-thin and Compton-thick material ($n_{\rm H_{torus}} = 10^{24}$atm cm^{-2}, red line), and the Compton-thick case ($n_{\rm H_{torus}} = 10^{25}$atm cm^{-2}, orange line). We confirm the findings from Murphy & Yaqoob (2009, 2011): the reprocessed Compton hump begins to appear for column densities of 10^{24}atm cm^{-2} and higher. This has an impact on the intensity and polarization spectra, in the sense that the higher densities induce a larger number of scattering events, hence an increase of the polarization in the hard X-ray band. However, the enhanced number of scattering implies a photon polarization angle that aligns more with a perfectly parallel orientation. This is why the energy-dependent variations of the polarization angle at high energies tend to be smoothed out. The soft X-ray band is less affected since photoabsorption is stronger than scattering probabilities.

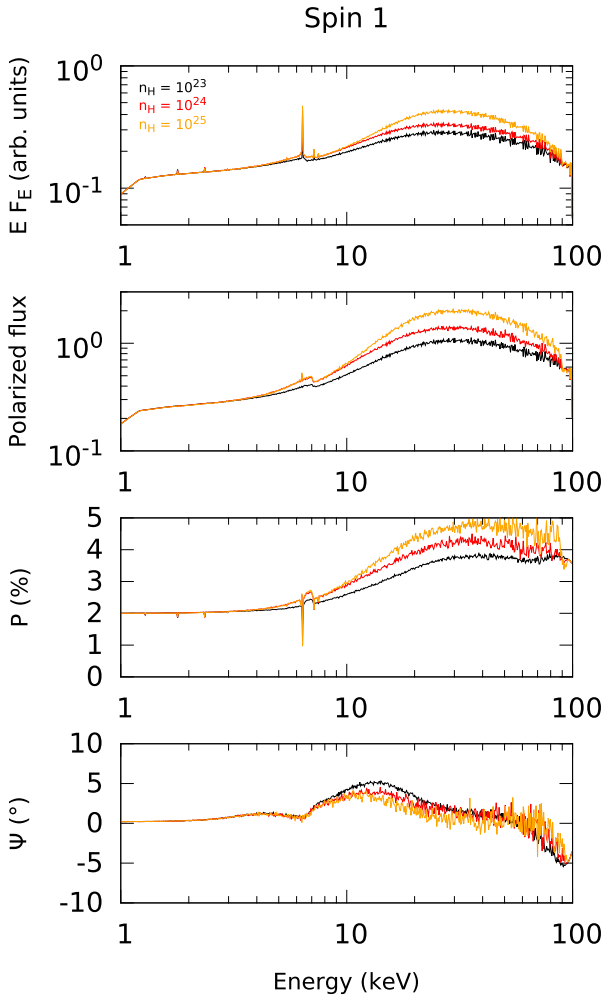

Figure 8. X-ray flux (F_E is energy flux at energy E), polarized flux, polarization degree, and polarization position angle for three type 1 AGN models with different torus Compton thickness: $n_{\rm H_{torus}} = 10^{23}$atm cm^{-2} (black), 10^{24}atm cm^{-2} (red), and 10^{25}atm cm^{-2} (orange). The polar winds are Compton-thin ($n_{\rm H_{wind}} = 10^{21}$atm cm^{-2}), and the input corona spectrum is 2 per cent parallelly polarized.

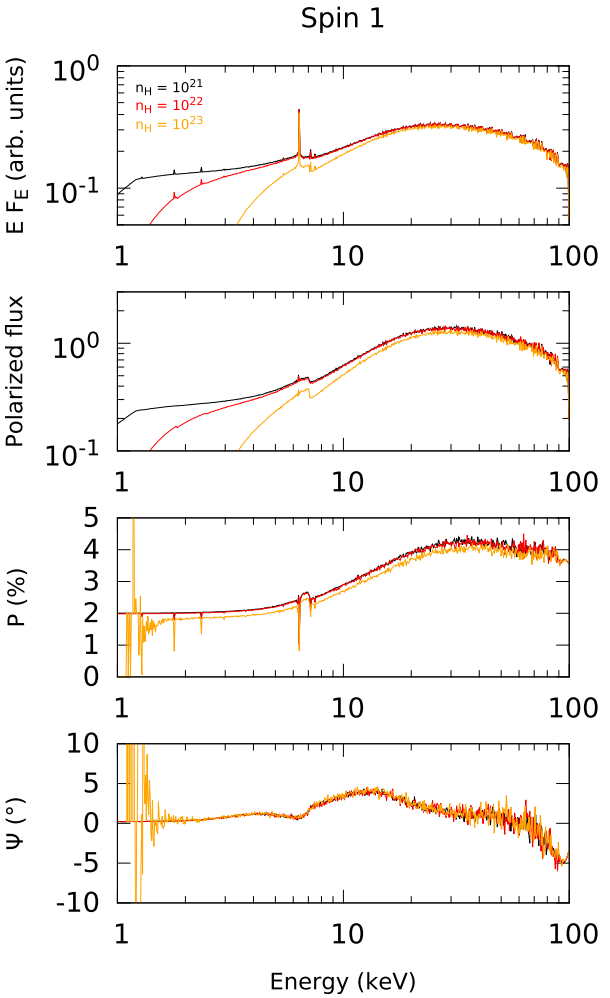

Figure 9. X-ray flux (F_E is energy flux at energy E), polarized flux, polarization degree, and polarization position angle for three type 1 AGN models with different wind Compton thickness: $n_{\rm H_{wind}} = 10^{21}$atm cm^{-2} (black), 10^{22}atm cm^{-2} (red), and 10^{23}atm cm^{-2} (orange). The torus is Compton-thick ($n_{\rm H_{torus}} = 10^{24}$atm cm^{-2}) and the input corona spectrum is 2 per cent parallelly polarized.

We thus see that the hard X-ray ($E \geq 10$ keV) polarization of type 1 Seyfert galaxies is influenced by parsec-scale equatorial regions. The polarization degree will be higher for higher hydrogen column densities but the disc–corona system signatures will be ultimately washed out by Compton-thick material along the equatorial plane. The soft X-ray band is less affected by the amount of molecular gas in the torus. In principle it could be feasible to determine the equivalent equatorial hydrogen density by measuring the X-ray polarization in the soft and hard bands, given the fact that the model is not too degenerated and that the polarimetric instrument is sensitive enough.

4.2 Impact of wind thickness

The second potential impacting parameter is the hydrogen column density along the observer's line-of-sight. This is represented in the form of the polar outflow in our AGN model and we disregard additional Galactic absorption since it will only contribute to decrease the observed flux (forward scattering is negligible). We thus vary the Compton thickness of the outflows in the model presented in Section 6. In Fig. 9 we test three column densities: $n_{\rm H_{wind}} = 10^{21}$atm cm^{-2} (black line), 10^{22}atm cm^{-2} (red line), and 10^{23}atm cm^{-2} (orange line). This is the typical range of X-ray column density for Seyfert galaxies as indexed by Jiménez-Bailón et al. (2008) and Fischer et al. (2014), the only exceptions being the uncommon windless, bare, AGN (Reeves et al. 2016; Porquet et al. 2018). We note that, for the case of Ark 120, the warm absorber region is seen in emission (Reeves et al. 2016), which indicates that the biconical configuration we use is a simplification and that the geometry of the polar component might be more complex, including the presence of hollow winds and clumps. These different configurations have already been addressed in Marin & Goosmann (2013) and Marin et al. (2015), respectively. In the case of uniformly filled conical winds, we observe that the higher the column density, the higher the absorbed flux in intensity. Additional molecular material leads to higher absorption probabilities (Odaka et al. 2016), but the impact on the polarization spectrum only appears for hydrogen column densities above 10^{23}atm cm^{-2}. The final po-

larization degree decreases due to two cumulative effects. First, fewer photons reach the observer, being scattered away from the observer's line-of-sight, resulting in strong statistical noise below 2 keV. Second, a non-negligible fraction of photons that were out of the line-of-sight start to scatter towards the observer when the hydrogen column density becomes high enough to collimate radiation in a sort of symmetric wind. The resulting photons acquire a random polarization, eventually contributing to the decrease of the final polarization degree we observe. Regarding Ψ, with the exception of numerical noise, the polarization position angle spectrum appears non-altered since transmission remains the dominant mechanism.

We conclude that varying the amount of gas in the polar direction has a deeper impact on the total flux spectrum than on the polarized component of light. The higher the X-ray column density, the lower the resulting polarization degree, but this diminution is almost constant in energy and is of the order of 0.1 percentage point for the cases studied here. The polarization position angle is completely unaffected.

5 CONCLUSIONS

We have tested whether old simulations of type 1 AGN that only considered the disc–corona system were reliable for predicting the X-ray polarization of type 1 radio-quiet AGN. We found that they do give a correct estimation of the order of magnitude of expected polarization but the addition of parsec-scale components, such as the equatorial circumnuclear region or polar outflows, has an impact. Depending on the initial polarization state of the X-ray photons produced in the corona, different outcomes may occur.

(i) If the initial photons are unpolarized or polarized parallelly to the accretion disc. In that case the polarization degree is almost unaffected below 3 keV, P increases by 0.1–0.5 percentage points between 3 and 10 keV, and the polarization degree is 0.5–1 percentage points higher at higher energies. The dominant contributor to those changes is the parsec-scale torus that adds a parallelly polarized component to the polarization of the central engine. The final polarization position angle is not strongly affected, but the energy-dependent variations of Ψ are smoothed out by the additional equatorial scattering contribution.

(ii) If the initial photons are polarized perpendicularly to the accretion disc. In that case the true polarization we expect to observe in type 1 AGN is lower by 0.1–0.5 percentage points between 3 and 10 keV with respect to what was predicted before when the central engine was isolated. Around 10 keV the polarization position angle rotates by 90° but at a slightly lower energy than in previous estimations. Finally, at $E \geq$ 10 keV, the total polarization degree is 0.5–1 percentage points higher than predicted. All these differences are due to the torus scattered component that adds some polarized flux at all energies with parallel polarization. The torus polarization adds to the central engine polarization above 10 keV, decreases polarization below 10 keV, and shifts the transition of the polarization position angle to lower energies.

Overall it is possible to correct previous simulations that did not account for extra parsec-scale AGN regions by simply increasing or decreasing the predicted degree of polarization. The polarization position angle is less affected, except regarding the energy at which the rotation of Ψ is expected if the corona produces perpendicularly polarized photons.

Our simulations are encouraging for the future of X-ray polarimetry since they predict slightly higher polarization degree than expected. This means that the amount of time needed to detect the polarization threshold will be lower for several AGN. As an example, in the case of NGC 3783 whose X-ray flux in the 2–10 keV band varies in the range 4–9 $\times$ 10^{-11} erg cm^{-2} s^{-1} (Kaspi et al. 2001), previous simulations would have require a 1.8 Ms observation for a *XIPE*-like S-class mission (Marin et al. 2012a), while, accounting for reprocessing on parsec-scale AGN components, the new estimation is slightly less than 1.2 Ms. We also see that detecting AGN polarization will be slightly easier than expected in the hard X-ray band due to enhanced Compton scattering. We thus strongly advocate for future X-ray polarimetric missions targeting both the soft and hard bands.

ACKNOWLEDGEMENTS

The authors would like to thank the anonymous referee for useful comments and suggestions. We are also grateful to Delphine Porquet for her numerous comments that helped to clarify and improve the text. This research has been supported by the Centre national d'études spatiales (CNES) thanks to the post-doctoral grant 'Probing the geometry and physics of active galactic nuclei with ultraviolet and X-ray polarized radiative transfer'. MD thanks for the support to MEYS INTER-INFORM LTI17018 project.

REFERENCES

Chandrasekhar S., 1960, Radiative Transfer. Dover, New York
Chartas G., Kochanek C. S., Dai X., Poindexter S., Garmire G., 2009, ApJ, 693, 174
Connors P. A., Stark R. F., Piran T., 1980, ApJ, 235, 224
Done C., Davis S. W., Jin C., Blaes O., Ward M., 2012, MNRAS, 420, 1848
Dovčiak M., Done C., 2016, Astron. Nachr., 337, 441
Dovčiak M., Karas V., Matt G., 2004a, MNRAS, 355, 1005
Dovčiak M., Karas V., Yaqoob T., 2004b, ApJS, 153, 205
Dovčiak M., Muleri F., Goosmann R. W., Karas V., Matt G., 2008, MNRAS, 391, 32
Dovčiak M., Muleri F., Goosmann R. W., Karas V., Matt G., 2011, ApJ, 731, 75
Dumont A.-M., Abrassart A., Collin S., 2000, A&A, 357, 823
Emmanoulopoulos D., Papadakis I. E., Dovčiak M., McHardy I. M., 2014, MNRAS, 439, 3931
Fabian A. C., Lohfink A., Belmont R., Malzac J., Coppi P., 2017, MNRAS, 467, 2566
Fabian A. C., Lohfink A., Kara E., Parker M. L., Vasudevan R., Reynolds C. S., 2015, MNRAS, 451, 4375
Fischer T. C., Crenshaw D. M., Kraemer S. B., Schmitt H. R., Turner T. J., 2014, ApJ, 785, 25
Gallo L. C. et al., 2015, MNRAS, 446, 633
Georgakakis A. et al., 2017, MNRAS, 469, 3232
Ghisellini G., Haardt F., Matt G., 1994, MNRAS, 267, 743
Goosmann R. W., Gaskell C. M., 2007, A&A, 465, 129
Haardt F., Maraschi L., 1991, ApJ, 380, L51
Haardt F., Maraschi L., 1993, ApJ, 413, 507
Haardt F., Matt G., 1993, MNRAS, 261, 346
Jiménez-Bailón E., Guainazzi M., Matt G., Bianchi S., Krongold Y., Piconcelli E., Santos Lleó M., Schartel N., 2008, Rev. Mex. Astron. Astrofis. Conf. Ser., 32, 131
Kaspi S. et al., 2001, ApJ, 554, 216
Marin F., 2016, MNRAS, 460, 3679
Marin F., 2018, preprint (arXiv:1805.09098)
Marin F., Dovčiak M., Muleri F., Kislat F. F., Krawczynski H. S., 2018, MNRAS, 473, 1286
Marin F., Goosmann R. W., 2013, MNRAS, 436, 2522
Marin F., Goosmann R. W., 2014, in Ballet J., Martins F., Bournaud F., Monier R., Reylé C., eds, SF2A-2014: Proceedings of the Annual Meet-

ing of the French Society of Astronomy and Astrophysics. Société Francaise d'Astronomie et d'Astrophysique (SF2A), Paris, p. 103
Marin F., Goosmann R. W., Dovčiak M., Muleri F., Porquet D., Grosso N., Karas V., Matt G., 2012a, MNRAS, 426, L101
Marin F., Goosmann R. W., Gaskell C. M., 2015, A&A, 577, A66
Marin F., Goosmann R. W., Gaskell C. M., Porquet D., Dovčiak M., 2012b, A&A, 548, A121
Marin F., Tamborra F., 2014, Adv. Space Res., 54, 1458
Massaro E., Matt G., Perola G. C., Costa E., Piro L., Soffitta P., 1993, A&AS, 97, 399
Matt G., Tamborra F., 2018, Galaxies, 6, 32
Matt G. et al., 2015, MNRAS, 447, 3029
Mosquera A. M., Kochanek C. S., Chen B., Dai X., Blackburne J. A., Chartas G., 2013, ApJ, 769, 53
Murphy K. D., Yaqoob T., 2009, MNRAS, 397, 1549
Murphy K. D., Yaqoob T., 2011, MNRAS, 415, 3962
Nayakshin S., Kallman T. R., 2001, ApJ, 546, 406
Odaka H., Yoneda H., Takahashi T., Fabian A., 2016, MNRAS, 462, 2366
Porquet D., Dubau J., 2000, A&AS, 143, 495
Porquet D. et al., 2018, A&A, 609, A42
Reeves J. N., Porquet D., Braito V., Nardini E., Lobban A., Turner T. J., 2016, ApJ, 828, 98
Reis R. C., Miller J. M., 2013, ApJ, 769, L7
Reynolds C. S., Fabian A. C., 1995, MNRAS, 273, 1167
Ricci C., Ueda Y., Ichikawa K., Paltani S., Boissay R., Gandhi P., Stalevski M., Awaki H., 2014, A&A, 567, A142
Rojas Lobos P. A., Goosmann R. W., Marin F., Savić D., 2018, A&A, 611, A39
Sądowski A., Bursa M., Abramowicz M., Kluźniak W., Lasota J.-P., Moderski R., Safarzadeh M., 2011, A&A, 532, A41
Schnittman J. D., Krolik J. H., 2010, ApJ, 712, 908
Schurch N. J., Done C., 2007, MNRAS, 381, 1413
Schurch N. J., Done C., Proga D., 2009, ApJ, 694, 1
Suganuma M. et al., 2006, ApJ, 639, 46
Taniguchi Y., Anabuki N., 1999, ApJ, 521, L103
Tombesi F., Cappi M., Reeves J. N., Braito V., 2012, MNRAS, 422, L1
Tombesi F., Cappi M., Reeves J. N., Palumbo G. G. C., Braito V., Dadina M., 2011, ApJ, 742, 44
Tombesi F., Cappi M., Reeves J. N., Palumbo G. G. C., Yaqoob T., Braito V., Dadina M., 2010, A&A, 521, A57
Tortosa A., Bianchi S., Marinucci A., Matt G., Petrucci P. O., 2018, preprint (arXiv:1801.04456)
Vazquez B. et al., 2014, Am. Astron. Soc. Meeting Abstr., 223, 251.04
Wang J., Xu D. W., Wei J. Y., 2016, AJ, 151, 81
Weisskopf M. C. et al., 2016, Proc. SPIE, 9905, 990517
Wilkins D. R., Fabian A. C., 2012, MNRAS, 424, 1284
Woo J.-H., Urry C. M., 2002, ApJ, 581, L5
Zamorani G., Gioia I. M., Maccacaro T., Wolter A., 1988, A&A, 196, 39
Zoghbi A., Fabian A. C., Uttley P., Miniutti G., Gallo L. C., Reynolds C. S., Miller J. M., Ponti G., 2010, MNRAS, 401, 2419

This paper has been typeset from a TEX/LATEX file prepared by the author.